Journal of Materials Chemistry A

Accepted Manuscript

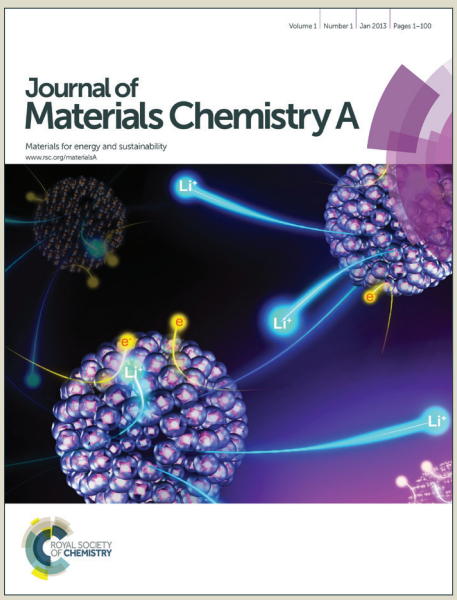

ROYAL SOCIETY OF CHEMISTRY

www.rsc.org/materialsA

Band-gap tuning of lead halide perovskites using a sequential deposition process

Sneha A. Kulkarni,*[a] Tom Baikie,[a] Pablo P. Boix,[a] Natalia Yantara,[a] Nripan Mathews, *[abc] Subodh Mhaisalkar [ab]

[a] Energy Research Institute @NTU (ERI@N), Research Techno Plaza, X-Frontier Block, Level 5, 50 Nanyang Drive, Singapore 637553.

[b] Nanyang Link, 637371 Singapore. 2School of Materials Science and Engineering, NTU, Nanyang Avenue, Singapore 639798

[c] Singapore-Berkeley Research Initiative for Sustainable Energy, 1 Create Way, Singapore 138602.

---

* Corresponding author. E-mail: Sakulkarni@ntu.edu.sg (S.A.K.); Nripan@ntu.edu.sg (N.M.)

Abstract

Band-gap tuning of mixed anion lead halide perovskites (*MA*Pb $(I_{1-x}Br_x)_3$ $(0 \leq x \leq 1)$ has been demonstrated by means of a sequential deposition process. The optical properties of perovskite hybrids can be flexibly modified by changing (mixing) the concentration of halogen precursors. The concentrations of precursor solution as well as the conversion time play an important role in determining the band-gap of perovskite. A systematic shift of the absorption band edge to shorter wavelengths is observed with increasing Br content in the perovskite films, which results in the decrement of the photocurrent. Nanorod like morphological features are also observed for perovskite films for iodide to bromide molar ratio <0.7.

Recently, organic-inorganic lead halide perovskites have attracted enormous attention as a photovoltaic material[1-4] due to their good electrical[5, 6] and optical properties[7-10], as well as their solution processability.[11-23] Initial efforts were made by using organolead halide perovskites as a sensitizer in dye sensitized solar cells (DSCs).[1] However, due to dissolution of the perovskite in the electrolyte, the performance degraded rapidly.[24] Subsequently, a power conversion efficiency (PCE) of 9.7% was reported for solid-state mesoscopic solar cells employing $CH_3NH_3PbI_3$.[25]

In the initial solid state reports, the perovskite layers were deposited using a single-step deposition from a solvent. However, the application of double-step procedure (involving the infiltration of the TiO_2 mesoporous layer with PbI_2 and subsequent in-situ conversion to $CH_3NH_3PbI_3$) has resulted in a record PCE of 15%.[26] In addition to the impressive efficiencies, an attractive feature of these classes of materials is the facile band-gap tunability, achievable through appropriate halide substitutions, resulting in an array of translucent colours. The mixed halide perovskite has been proposed to be more chemically stable than pure $CH_3NH_3PbI_3$, which decomposes to PbI_2 under humid conditions. [4, 26] Typically, perovskite structure consists of a three-dimensional network of corner-corner connected MX_6 octahedra, where *M* (metal) cation is located at the centre of the octahedra and *X* (Cl, Br, I) lies in the corners around *M*. Computational calculations for mixed perovskite systems show the existence of two different types of structures with different electronic properties whose relative stability varies by varying the contribution of '*X*' as well as their position in octahedra (*X* = Cl, Br, I). [27] In case of the mixed halide perovskites, for instance, in MI_4X_2 (*X*=Cl or Br) octahedra, Cl atoms preferentially occupy the apical positions, while the Br atom may occupy apical sites as well as equatorial positions. However, this would imply the mixed anion perovskites adopt non-cubic symmetry. The variation in the composition of the halides in the lead perovskites modulates their optical

properties, which directly influences the light harvesting capability of the photoanode and thus the short-circuit photocurrent density of the device.[27] In the previous report on band-gap tunable mixed halide perovskites for solar cells applications, the perovskite films were prepared using a single step deposition process.[26] Here, we demonstrate the adaptation of sequential deposition process to enable band-gap tuning of the mixed halide perovskite sensitizer. A film of lead iodide (PbI_2) was first deposited onto mesoporous (mp)-TiO_2/bl-TiO_2/FTO substrate using spin-coating. The spin-coated films were subsequently annealed and after cooling were dipped into a mixed methyl ammonium iodide (*MA*I)/ methyl ammonium bromide (*MA*Br) (V/V) solutions in isopropanol (subsequently molar concentrations were calculated) to form the mixed perovskites. Detailed characterization of the perovskite films were carried out using optical absorption spectroscopy, X-ray diffraction (XRD) and Field emission scanning electron microscopy (FE-SEM). The photovoltaic device performances of the mixed halide perovskite systems were characterized in detail indicating high efficiency is possible by optimizing fabrication parameters.

Results and Discussion

In the sequential deposition process, two different approaches can be used to tune the band-gap of the mixed halide perovskites: Fixing the molar ratio of the mixed halide (i.e. *MA*I: *MA*Br) solution while varying the dipping time of PbI_2 film, and varying the molar ratios of the mixed halide solutions whilst dipping the PbI_2 films for a constant time period. In the first approach, the dipping time of the PbI_2 films in the mixture of *MA*I & *MA*Br was varied from 30 sec to 20 minutes. Ex-situ UV measurements for various dipping times were carried out to estimate the band gap of the films. The estimated band-gap for the standard *MA*PbI_3 perovskite films (formed by dipping the PbI_2 film only in pure *MA*I solution) were noted to be invariant with respect to dipping time with an observed band-gap of 1.56 eV consistent with earlier reports (Supporting

information: Fig.S1 (A)). For PbI_2 films dipped in the 1:1 mixture of MAI: MABr, a band-gap variation from 1.69 eV to 1.82 eV is observed at different dipping time intervals. The band-gap subsequently stabilized at 1.75 eV after 20 minutes of dipping time (Supporting information: Fig.S1 (B)). This may be due to the relative stability of the perovskite formed at particular time interval, which is mainly dependent on the contribution of '*X*' (*X*= I & Br) as well as position of X in the octahedral. Another factor to be considered is the relative solubility of halide perovskites in the isopropanol solution. Interestingly, a clear blue shift in the absorption band-edge is observed for the perovskite films formed by dip coating the PbI_2 films in pure *MA*Br solution for different time intervals. Analysis of such perovskite films formed at 0.5min, 5mins, 10mins & 20 mins dipping time interval indicates an absorption edge of 660 nm, 645 nm, 625 nm & 556 nm corresponding to band-gaps of 1.89 eV, 1.92 eV, 1.98 eV & 2.23 eV respectively (Supporting information Fig. S1: (C)). Thus a systematic band-gap shift to the wider band-gap region is observed with respect to dipping time in pure bromide precursor indicating that band-gap tuning is possible by controlling the composition of the halide precursor and varying the dipping time interval of metal halide film in the precursor solution. In addition, as per optical absorption measurements, it is also noted that the 15-20 minutes dipping time interval is needed for complete transformation of perovskite to a stable composition.

In order to evaluate the effect of the concentration, the PbI_2 films were dipped at a fixed time interval i.e. ~20 minutes into the various molar compositions of the halide precursor solutions. For ease of experimentation, the solutions were prepared by varying the volume ratio of *MA*I and *MA*Br for a known concentration. The UV-Vis absorption spectra of $MAPb(I_{1-x}Br_x)_3$ ($0 \leq x \leq 1$) perovskite films on mp-TiO_2/bl-TiO_2/FTO substrates are shown in Figure 1, where '*x*' indicates the amount of *MA*Br (in mole) in the mixture of *MA*I and *MA*Br solution. The onset of the

absorption band is observed to shift to the lower wavelength region with increasing *MA*Br content in the mixed solvent i.e. from 794 nm (1.57 eV) for pure iodide based perovskite to 556 nm (2.23 eV) for the bromide rich mixed halide perovskites. As a result, the color of the $MAPbI_3$ perovskite films were observed to change from dark brown/black to red to orange (Fig. 1, insert photographs (1 to 7)) with increasing bromide content. The band-gaps extracted from the optical absorption measurements are listed in Table 1 along with their estimated *MA*I:*MA*Br molar ratios and the respective compositions in the mixed halide perovskite films. The composition of halides in perovskite films were estimated based on their measured band-gap values as per the following relation, $Eg(x) = 1.57 + 0.39x + 0.33x^2$, where *Eg* is the band gap of the perovskite in eV and *x* is the amount of Br relative to the amount of I.[26] It is to be noted that the estimated halide composition in the perovskite film is different from the initial *MA*I and *MA*Br precursor composition, which is probably due to the additional contribution of iodide from the lead iodide precursor.

X-ray diffraction spectra shown in Figure 2 provides further confirmation that the sequential deposition process is successful in producing the mixed Br/I perovskites, and Pawley fits of the diffraction data confirmed the lattice parameters varied appropriately when the smaller Br^- (IR = 1.96 Å) ion substitutes the I^- (IR = 2.2 Å) (see Figure 2a and b). The (004) and (220) of the tetragonal phase merge upon increasing bromide content (*x*) to a Bragg reflection corresponding to the (200) reflection of the cubic phase at around $x = 0.2$. Together with the perovskite phase, diffraction reflections consistent with TiO_2 and FTO were identified in all diffraction phase and were modelled with their respective reported structural information. (Fig. S2 and Table S1) In addition, as reported in the previous work the 00l reflections for the 2*H* polymorph of PbI_2 was often identified in the prepared thin films, which may indicate incomplete conversion to

perovskite phase or slight sample decomposition.[19] Also consistent with previous work the exchange of I^- for Br^- is in fairly close agreement with Vegard's law but the slight deviation from this trend at higher Br^- content, may suggest there is a small miscibility gap, a site preference for the bromide in the perovskite octahedra, or further variations in symmetry as Br^- substitutes I^-. [26] [27] This latter effect is currently under further investigation via the preparation and the study of the single crystal mixed-anion perovskites, and will be reported elsewhere. The crystallite size of the perovskite phases were estimated using the Scherrer equation, and indicated the perovskite component of the thin films had crystallite sizes of approximately 20-30 nm.

Table 2 illustrates the photovoltaic characteristic parameters for perovskite devices prepared by dipping PbI_2/mp-TiO_2/bl-TiO_2/FTO substrates in the mixture of MAI: MABr in the various molar ratios for a 20 minute time interval. The corresponding normalized IPCE data are shown in Figure 3. The obtained efficiency for best devices fabricated with $MAPbI_3$ and *MA*Pb $(I_{0.05}Br_{0.95})_3$ were 12.04 % and 1.58 % respectively. The characteristic I-V curves are shown in supporting information (Fig. S3). Although these values are lower than previous reports, optimization of the device fabrication conditions (for eg, increasing the TiO_2 thickness or the PbI_2 loading for perovskites with low optical absorption coefficients) were not performed as it is not the focus of the present work. A reduction in the J_{sc} is noted with increasing Br content in the perovskite films, due to the increased band gap which results in the blue-shift of absorption onset. It has been reported that the charge transport and recombination behavior of *MA*Pb $(I_{1-x}Br_x)_3$ were greatly changed near x=0.58 in *MA*Pb $(I_{1-x}Br_x)_3$, although the $MAPb(I_{1-x}Br_x)_3$ compound was uniformly formed in the entire range.[26]

Figure 4 shows the FESEM images of the top (first row) and cross sectional views (second row) of films with different perovskite compositions namely a) *MA*PbI_3 b) *MA*$Pb(I_{0.59}Br_{x0.41})_3$ c)

*MA*Pb($I_{0.15}Br_{0.85}$)$_3$ and d) *MA*$PbBr_3$. The FESEM images (top and cross-sectional views) of the perovskite films with different bromide content are shown in supporting information (Fig.S4). The film formed with *MAPbI$_3$* composition shows uniform perovskite formation with a thickness of approximately 180 nm. In the mixed halide perovskite films, the increasing Br content results in crystallites with alternative faceting, which reflects the change in crystal structure from tetragonal to cubic symmetry. The length of crystals varies (220nm-320nm) with the Br content in the perovskite film, resulting in nanorod like morphological features. Such crystal growth is observed for perovskite films with bromide contribution > 40 %. The reduction in the solar cell efficiencies with increasing bromide concentration, may also be attributable to such rough morphologies which result in poor coverage by the hole transport layer. The process parameters such as perovskite formation time, hole transport material concentration/deposition conditions (due to different morphological features) are needed to be optimised to achieve an improved device performance.

Conclusions:

Band-gap tuning of perovskite films has been demonstrated by means of a sequential deposition method. The PbI_2 film dipping time in halide precursors as well as the concentration of halide precursors is noted to play a crucial role in determining the composition and thus the band-gap of the mixed halide perovskites. The incident photon to current efficiency (IPCE) clearly shows the systematic shifts towards lower wavelengths with increasing Br content in the perovskite films, in agreement with optical absorption measurements. The modulation of the bandgap is accompanied by morphological evolution as well.

Acknowledgement:

Funding from National Research Foundation (NRF), Singapore, is acknowledged through CRP

Award No.: NRF-CRP4-2008-03 and the Singapore-Berkeley Research Initiative for Sustainable Energy (SinBeRISE) CREATE programme.

Notes
The authors declare no competing financial interest.

References

1. A. Kojima, K. Teshima, Y. Shirai and T. Miyasaka, *Journal of the American Chemical Society*, 2009, **131**, 6050-6051.
2. I. Chung, B. Lee, J. He, R. P. H. Chang and M. G. Kanatzidis, *Nature*, 2012, **485**, 486-489.
3. M. Liu, M. B. Johnston and H. J. Snaith, *Nature*, 2013, **501**, 395-398.
4. M. M. Lee, J. Teuscher, T. Miyasaka, T. N. Murakami, H. J. Snaith and J. Henry, *Science (New York, N.Y.)*, 2012, **643**, 1-7.
5. D. B. Mitzi, C. A. Feild, W. T. A. Harrison and A. M. Guloy, *Nature*, 1994, **369**, 467-469.
6. D. B. Mitzi, S. Wang, C. A. Feild, C. A. Chess and A. M. Guloy, *Science*, 1995, **267**, 1473-1476.
7. D. B. Mitzi, C. A. Feild, Z. Schlesinger and R. B. Laibowitz, *Journal of Solid State Chemistry*, 1995, **114**, 159-163.
8. T. Ishihara, J. Takahashi and T. Goto, *Physical Review B*, 1990, **42**, 11099-11107.
9. N. Kitazawa, *Materials Science and Engineering: B*, 1997, **49**, 233-238.
10. S. Zhang, P. Audebert, Y. Wei, A. Al Choueiry, G. t. Lanty, A. Brehier, L. Galmiche, G. Clavier, C. d. Boissiere, J.-S. b. Lauret and E. Deleporte, *Materials* 2010, **3(5)** 3385-3406.
11. G. Xing, N. Mathews, S. Sun, S. S.Lim, Y. M. Lam, M. Grätzel, S. Mhaisalkar and T. C. Sum, *Science*, 2013, **342 (6156),** , 344-347.
12. J. Burschka, N. Pellet, S.-J. Moon, R. Humphry-Baker, P. Gao, M. K. Nazeeruddin and M. Gratzel, *Nature*, 2013, **499**, 316-319.
13. M. J. Carnie, C. Charbonneau, M. L. Davies, J. Troughton, T. M. Watson, K. Wojciechowski, H. Snaith and D. A. Worsley, *Chemical communications (Cambridge, England)*, 2013.
14. M. H. Kumar, N. Yantara, S. Dharani, M. Graetzel, S. Mhaisalkar, P. P. Boix and N. Mathews, *Chemical Communications*, 2013.
15. D. Sabba, H. M. Kumar, N. Yantara, T. T. T. Pham, N.-G. Park, M. Gratzel, S. G. Mhaisalkar, N. Mathews and P. P. Boix, *Nanoscale*, 2013.
16. H.-S. Kim, J.-W. Lee, N. Yantara, P. P. Boix, S. A. Kulkarni, S. Mhaisalkar, M. Grätzel and N.-G. Park, *Nano Letters*, 2013, **13**, 2412-2417.
17. H.-s. Kim, I. Mora-Sero, V. Gonzalez-Pedro, F. Fabregat-Santiago, E. J. Juarez-Perez, N.-g. Park and J. Bisquert, *Nature Communications*, 2013, **4**, 1-7.
18. N.-G. Park, *The Journal of Physical Chemistry Letters*, 2013, 130711081114003-130711081114003.

19. T. Baikie, Y. Fang, J. M. Kadro, M. Schreyer, F. Wei, S. G. Mhaisalkar, M. Graetzel and T. J. White, *Journal of Materials Chemistry A*, 2013, **1**, 5628-5641.
20. J. H. Heo, S. H. Im, J. H. Noh, T. N. Mandal, C.-S. Lim, J. A. Chang, Y. H. Lee, H.-j. Kim, A. Sarkar, M. K. Nazeeruddin, M. Grätzel and S. I. Seok, *Nature Photonics*, 2013, 1-6.
21. W. E. I. Zhang, M. Saliba, S. D. Stranks, Y. Sun, X. Shi, U. Wiesner and H. J. Snaith, *Nano Letters*, 2013, 130815103150002-130815103150002.
22. L. Etgar, P. Gao, Z. Xue, Q. Peng, A. K. Chandiran, B. Liu, M. K. Nazeeruddin and M. Grätzel, *Journal of the American Chemical Society*, 2012, **134**, 17396-17399.
23. M. N. Xing Guichuan, Sun Shuangyong , Lim Swee Sien, Lam Yeng Ming , Grätzel Michael , Mhaisalkar Subodh , and Sum Tze Chien, *Science*, 2013, **342 (6156),** , 344-347.
24. J.-H. Im, C.-R. Lee, J.-W. Lee, S.-W. Park and N.-G. Park, *Nanoscale*, 2011, **3**, 4088-4093.
25. H.-S. Kim, C.-R. Lee, J.-H. Im, K.-B. Lee, T. Moehl, A. Marchioro, S.-J. Moon, R. Humphry-Baker, J.-H. Yum, J. E. Moser, M. Grätzel and N.-G. Park, *Scientific Reports*, 2012, **2**, 1-7.
26. J. H. Noh, S. H. Im, J. H. Heo, T. N. Mandal and S. I. Seok, *Nano Letters*, 2013, **13**, 1764-1769.
27. E. Mosconi, A. Amat, M. K. Nazeeruddin, M. Grätzel and F. De Angelis, *The Journal of Physical Chemistry C*, 2013, **117**, 13902-13913.

Table 1

Table 1: The variation in volume and molar ratio of *MA*I and *MA*Br, measured band gap values and estimated composition of halides (iodide/bromide) in the perovskite film, the composition is estimated using the equation [a] $Eg(x) = 1.57 + 0.39x + 0.33x$.

Film No.	MAI: MABr (V/V)	MAI: MABr (moles)	Measured band gap (eV)	[a] Estimated composition of films [26]
1	1:0	-	1.56	$MAPbI_3$
2	4:1	2.85	1.62	$MAPb(I_{0.88}Br_{0.12})_3$
3	2:1	1.42	1.69	$MAPb(I_{0.74}Br_{0.26})_3$
4	1:1	0.70	1.79	$MAPb(I_{0.58}Br_{0.42})_3$
5	1:2	0.35	1.96	$MAPb(I_{0.41}Br_{0.59})_3$
6	1:4	0.17	2.01	$MAPb(I_{0.28}Br_{0.72})_3$
7	0:1	-	2.23	$MAPb(I_{0.05}Br_{0.95})_3$

Table 2

Table 2: Characteristic photovoltaic parameters, photocurrent density (Jsc), open circuit voltage (Voc), fill factor (FF) and efficiency (η) of the mixed halide (iodide/bromide) perovskite device, prepared by dipping PbI_2/mp-TiO_2/bl-TiO_2/FTO substrate in the mixture of MAI:MABr for various (V/V) ratios at 20 minutes time interval. The average and standard deviation (s.d) values were calculated for four different batches of the devices fabricated under identical fabrication conditions

Film No.	Estimated halide composition in lead perovskite films	Jsc (mA/cm^2)	Voc (V)	FF (%)	η (%)
1	$MAPbI_3$	17.45 ± 1.48	0.977 ± 0.074	61.13 ± 1.81	10.64 ± 1.97
2	$MAPb(I_{0.88}Br_{0.12})_3$	13.89 ± 0.42	0.890 ± 0.092	65.31 ± 6.78	8.13 ± 0.91
3	$MAPb(I_{0.74}Br_{0.26})_3$	10.39 ± 1.58	0.936 ± 0.023	61.95 ± 1.70	6.13 ± 0.85
4	$MAPb(I_{0.58}Br_{0.42})_3$	8.20 ± 2.62	0.898 ± 0.028	65.84 ± 2.85	4.63 ± 1.49
5	$MAPb(I_{0.41}Br_{0.59})_3$	6.35 ± 0.55	0.834 ± 0.064	52.40 ± 1.83	2.80 ± 0.51
6	$MAPb(I_{0.28}Br_{0.72})_3$	3.18 ± 1.22	0.940 ± 0.135	48.54 ± 14.92	1.39 ± 0.98
7	$MAPb(I_{0.05}Br_{0.95})_3$	2.38 ± 0.37	0.832 ± 0.159	49.81 ± 6.67	1.03 ± 0.49

Figures 1

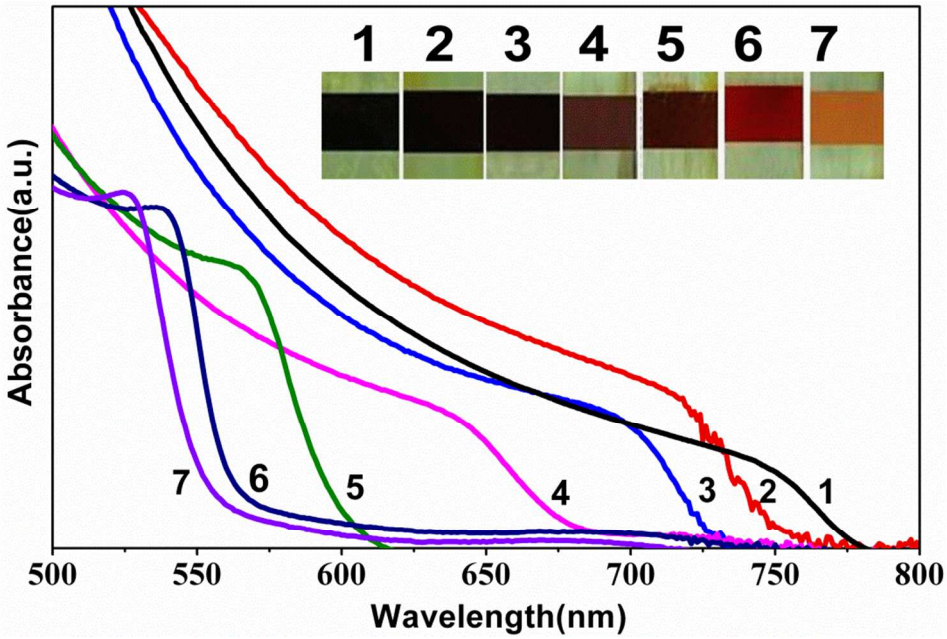

Fig.1: UV–Vis absorption spectra of the mixed halide lead perovskites (MAPb $(I_{1-x}Br_x)_3$ ($0 \leq x \leq 1$)) films formed via a sequential deposition process. The numbers 1-7 corresponds to the mixed lead halide perovskite films with different halide (iodide/bromide) composition as estimated in the corresponding table. Insert show the photographs of mixed lead halide nanocomposites perovskite films on FTO substrates.

Figures 2

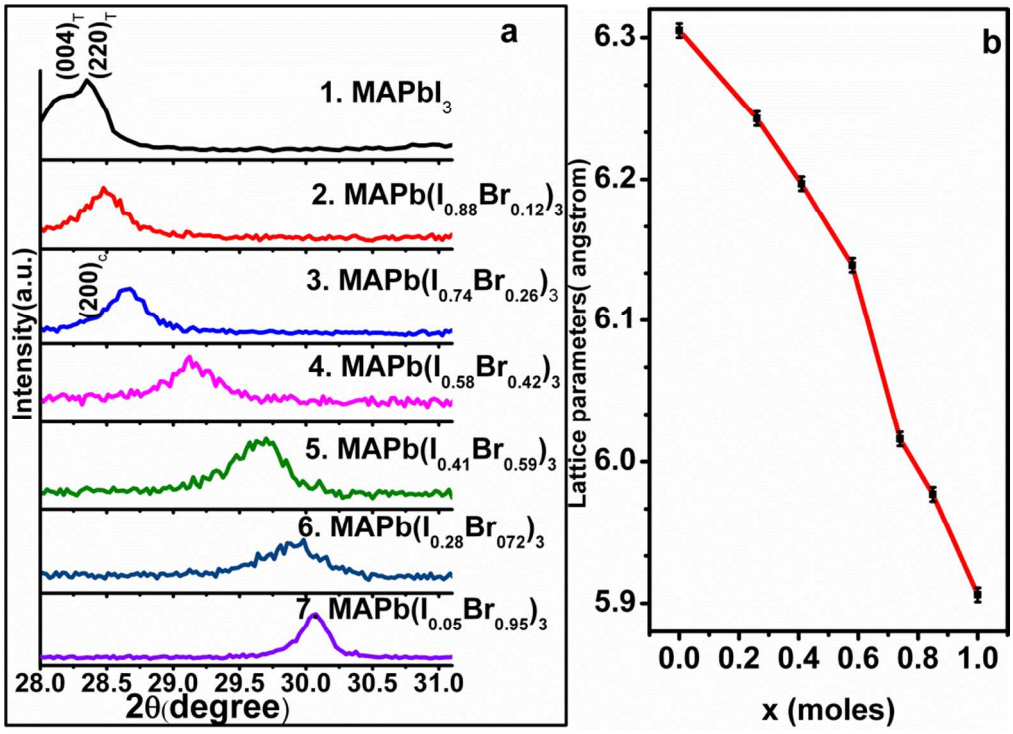

Fig.2 Powder X-ray diffraction analysis of mixed lead halide perovskite films *MA*Pb $(I_{1-x}Br_x)_3$ $(0 \leq x \leq 1)$ in the region of the tetragonal (004)T & (220)T and cubic (200)C reflections (2θ = 27.5−31.0°); (b) Lattice parameters of pseudocubic or cubic *MA*Pb$(I_{1-x}Br_x)_3$ as a function of Br content (x in moles) along with the precision of experimental data fitting.

Figures 3

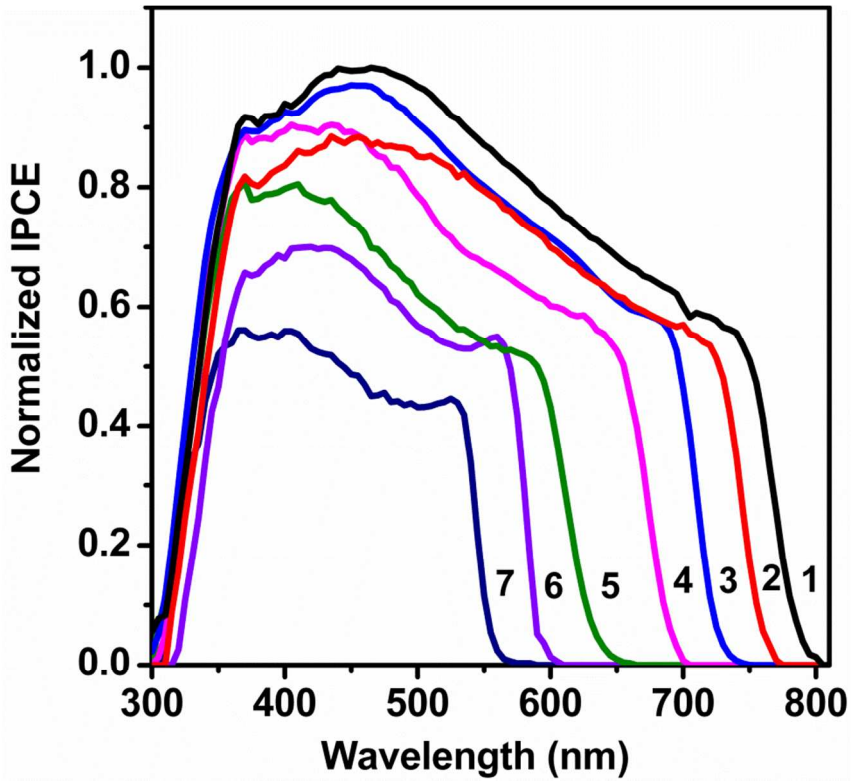

Fig.3: The normalised IPCE spectra of the mixed lead halide perovskite devices. The number 1 to 7 represents the composition of the mixed halide as represented in table 2.

Figures 4

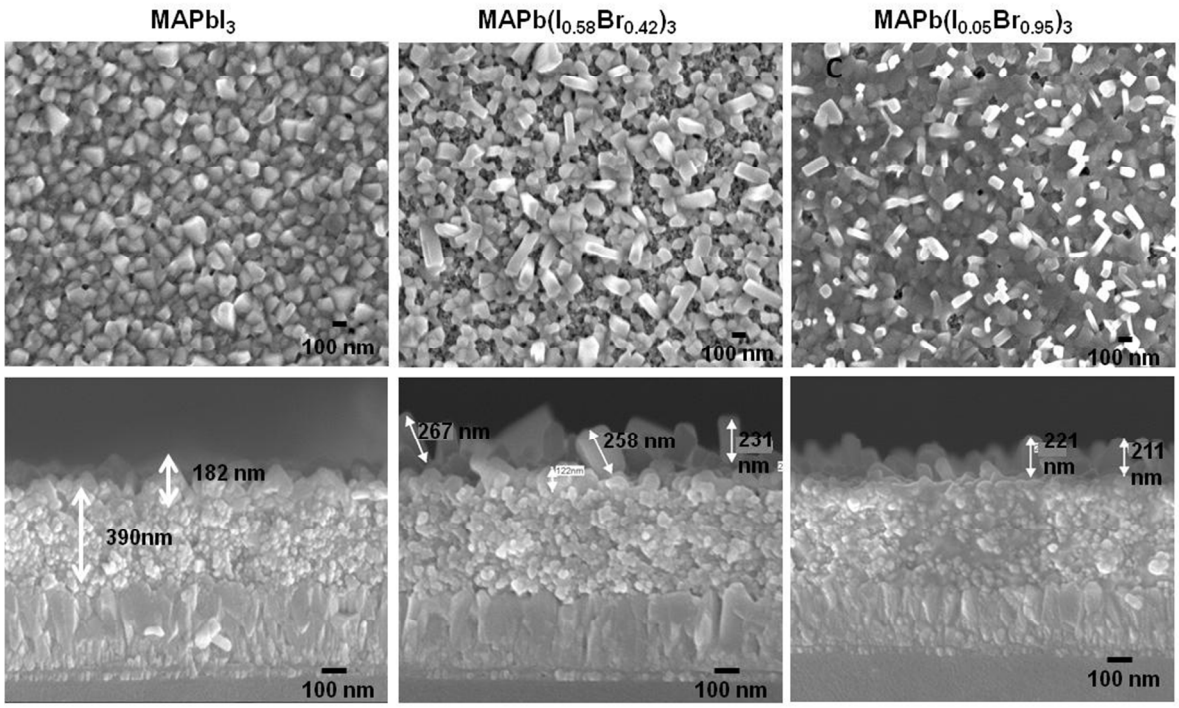

Fig. 4: Field emission microscopic (FESEM) images of mixed halide perovskite films with different halide namely; $MAPbI_3$, MAPb $(I_{0.58}Br_{x0.42})_3$ and MAPb $(I_{0.05}Br_{0.95})_3$ top (first row) and cross sectional view (second row).